

# Low $Q^2$ measurements of the proton form factor ratio $\mu_p G_E/G_M$

G. Ron,<sup>1,2,3</sup> X. Zhan,<sup>4</sup> J. Glistler,<sup>5,6</sup> B. Lee,<sup>7</sup> K. Allada,<sup>8</sup> W. Armstrong,<sup>9</sup> J. Arrington,<sup>10</sup> A. Beck,<sup>4,11</sup> F. Benmokhtar,<sup>12</sup> B.L. Berman,<sup>13</sup> W. Boeglin,<sup>14</sup> E. Brash,<sup>15</sup> A. Camsonne,<sup>11</sup> J. Calarco,<sup>16</sup> J. P. Chen,<sup>11</sup> Seonho Choi,<sup>7</sup> E. Chudakov,<sup>11</sup> L. Coman,<sup>17</sup> B. Craver,<sup>17</sup> F. Cusanno,<sup>18</sup> J. Dumas,<sup>19</sup> C. Dutta,<sup>8</sup> R. Feuerbach,<sup>11</sup> A. Freyberger,<sup>11</sup> S. Frullani,<sup>18</sup> F. Garibaldi,<sup>18</sup> R. Gilman,<sup>19,11</sup> O. Hansen,<sup>11</sup> D. W. Higinbotham,<sup>11</sup> T. Holmstrom,<sup>20</sup> C.E. Hyde,<sup>21</sup> H. Ibrahim,<sup>21</sup> Y. Ilieva,<sup>13</sup> C. W. de Jager,<sup>11</sup> X. Jiang,<sup>19</sup> M. Jones,<sup>11</sup> A. Kelleher,<sup>20</sup> E. Khrosinkova,<sup>22</sup> E. Kuchina,<sup>19</sup> G. Kumbartzki,<sup>19</sup> J. J. LeRose,<sup>11</sup> R. Lindgren,<sup>17</sup> P. Markowitz,<sup>14</sup> S. May-Tal Beck,<sup>4,11</sup> E. McCullough,<sup>5</sup> M. Meziane,<sup>20</sup> Z.-E. Meziani,<sup>9</sup> R. Michaels,<sup>11</sup> B. Moffit,<sup>20</sup> B.E. Norum,<sup>17</sup> Y. Oh,<sup>7</sup> M. Olson,<sup>23</sup> M. Paolone,<sup>24</sup> K. Paschke,<sup>17</sup> C. F. Perdrisat,<sup>20</sup> E. Piasetzky,<sup>25</sup> M. Potokar,<sup>26</sup> R. Pomatsalyuk,<sup>27,11</sup> I. Pomerantz,<sup>25</sup> A. J. R. Puckett,<sup>4</sup> V. Punjabi,<sup>28</sup> X. Qian,<sup>29</sup> Y. Qiang,<sup>4</sup> R. Ransome,<sup>19</sup> M. Reyhan,<sup>19</sup> J. Roche,<sup>30</sup> Y. Rousseau,<sup>19</sup> A. Saha,<sup>11</sup> A.J. Sarty,<sup>5</sup> B. Sawatzky,<sup>17,9</sup> E. Schulte,<sup>19</sup> M. Shabestari,<sup>17</sup> A. Shahinyan,<sup>31</sup> R. Shneur,<sup>25</sup> S. Širca,<sup>32,26</sup> K. Slifer,<sup>17</sup> P. Solvignon,<sup>10</sup> J. Song,<sup>7</sup> R. Sparks,<sup>11</sup> R. Subedi,<sup>22</sup> S. Strauch,<sup>24</sup> G. M. Urciuoli,<sup>33</sup> K. Wang,<sup>17</sup> B. Wojtsekhowski,<sup>11</sup> X. Yan,<sup>7</sup> H. Yao,<sup>9</sup> and X. Zhu<sup>34</sup>

(The Jefferson Lab Hall A Collaboration)

<sup>1</sup>The Weizmann Institute of Science, Rehovot 76100, Israel

<sup>2</sup>Lawrence Berkeley National Lab, Berkeley, CA 94720, USA

<sup>3</sup>Racah Institute of Physics, Hebrew University of Jerusalem, Jerusalem, Israel 91904

<sup>4</sup>Massachusetts Institute of Technology, Cambridge, Massachusetts 02139, USA

<sup>5</sup>Saint Mary's University, Halifax, Nova Scotia B3H 3C3, Canada

<sup>6</sup>Dalhousie University, Halifax, Nova Scotia B3H 3J5, Canada

<sup>7</sup>Seoul National University, Seoul 151-747, Korea

<sup>8</sup>University of Kentucky, Lexington, Kentucky 40506, USA

<sup>9</sup>Temple University, Philadelphia, Pennsylvania 19122, USA

<sup>10</sup>Argonne National Laboratory, Argonne, Illinois, 60439, USA

<sup>11</sup>Thomas Jefferson National Accelerator Facility, Newport News, Virginia 23606, USA

<sup>12</sup>University of Maryland, Baltimore, Maryland, USA

<sup>13</sup>George Washington University, Washington D.C. 20052, USA

<sup>14</sup>Florida International University, Miami, Florida 33199, USA

<sup>15</sup>Christopher Newport University, Newport News, Virginia, 2360X, USA

<sup>16</sup>University of New Hampshire, Durham, New Hampshire 03824, USA

<sup>17</sup>University of Virginia, Charlottesville, Virginia 22904, USA

<sup>18</sup>INFN, Sezione Sanità and Istituto Superiore di Sanità, Laboratorio di Fisica, I-00161 Rome, Italy

<sup>19</sup>Rutgers, The State University of New Jersey, Piscataway, New Jersey 08855, USA

<sup>20</sup>College of William and Mary, Williamsburg, Virginia 23187, USA

<sup>21</sup>Old Dominion University, Norfolk, Virginia 23508, USA

<sup>22</sup>Kent State University, Kent, Ohio 44242, USA

<sup>23</sup>Saint Norbert College, Greenbay, Wisconsin 54115, USA

<sup>24</sup>University of South Carolina, Columbia, South Carolina 29208, USA

<sup>25</sup>Tel Aviv University, Tel Aviv 69978, Israel

<sup>26</sup>Institute "Jožef Stefan", 1000 Ljubljana, Slovenia

<sup>27</sup>Kharkov Institute, Kharkov 310108, Ukraine

<sup>28</sup>Norfolk State University, Norfolk, Virginia 23504, USA

<sup>29</sup>Duke University, Durham, NC 27708, USA

<sup>30</sup>Ohio University, Athens, Ohio 45701, USA

<sup>31</sup>Yerevan Physics Institute, Yerevan 375036, Armenia

<sup>32</sup>Dept. of Physics, University of Ljubljana, 1000 Ljubljana, Slovenia

<sup>33</sup>INFN, Sezione di Roma, I-00185 Rome, Italy

<sup>34</sup>Duke University, Durham, North Carolina 27708, USA

(Dated: November 1, 2018)

We present an updated extraction of the proton electromagnetic form factor ratio,  $\mu_p G_E/G_M$ , at low  $Q^2$ . The form factors are sensitive to the spatial distribution of the proton, and precise measurements can be used to constrain models of the proton. An improved selection of the elastic events and reduced background contributions yielded a small systematic reduction in the ratio  $\mu_p G_E/G_M$  compared to the original analysis.

PACS numbers: 13.0.Gp, 13.60.Fz, 13.88.+e, 14.20.Dh

## I. INTRODUCTION

$\mu_p G_E/G_M$  initially presented in Ref. [1], with improved

We present a detailed reanalysis of polarization transfer measurements of the proton form factor ratio

selection of elastic events and significantly reduced contamination from quasielastic events in the target windows. The new results are typically lower by  $\sim 1\%$ .

The electric and magnetic form factors,  $G_E(Q^2)$  and  $G_M(Q^2)$ , describe the distribution of charge and magnetization in the proton. The form factors are extracted in elastic electron–proton scattering and mapped out as a function of the four-momentum transfer squared,  $Q^2$ , to yield the momentum-space structure of the proton. Precision measurements of proton form factors over a large kinematic range can provide important constraints on models of the proton. However, when extracting the form factors from unpolarized cross section measurements using the Rosenbluth separation technique, it is difficult to precisely separate  $G_E$  from  $G_M$  in the proton for very high or very low  $Q^2$  values. The addition of polarization measurements [2–5] allows for a much better separation of  $G_E$  and  $G_M$ . Initial measurements for the proton focused on the high- $Q^2$  region [6–10], which showed a significant falloff in the ratio  $\mu_p G_E/G_M$  with  $Q^2$ , in contrast to previous extractions from Rosenbluth separations [11]. This difference is now believed to be due to the contribution of two-photon exchange effects which have a large impact on the extractions from the unpolarized cross section measurements but have less impact on the polarization measurements [12–17]. These significantly improved measurements of  $G_E$  led to a great deal of theoretical work aimed at understanding this behavior [18–21], which showed, among other things, the importance of quark orbital angular momentum in understanding the proton structure at high momentum [22–24]. These results also had a significant impact on studies of the correlations between the spatial distribution of the quarks and the spin or momentum they carry, showing that the spherically symmetric proton is formed from a rich collection of complex overlapping structures [25].

While initial investigations focused on extending proton measurements to higher  $Q^2$ , the polarization measurements can also be used to improve extractions at low  $Q^2$  values, providing improved precision and less sensitivity to two-photon exchange corrections. The low- $Q^2$  form factors relate to large-scale structures in the proton’s charge and magnetization distributions. As such, it has long been believed that the “pion cloud” contributions, e.g. the fluctuation of a proton into a virtual neutron- $\pi^+$  system, will be important at low  $Q^2$ , as the mass difference means that the pion will contribute to the large distance distribution in the bound nucleon–pion system. It was recently suggested that such structures are present in all the nucleon form factors [26], centered at  $Q^2 \approx 0.3 \text{ GeV}^2$ , and that these structures reflect contributions from the pion cloud of the nucleon. However, the significance of the proposed structures and their interpretation as a pion cloud effect have been much disputed. This low- $Q^2$  region is also important in parity violating electron scattering measurements [27–30] aimed at investigating the strange-quark contributions to the proton electromagnetic structure. Isolating the strange

quark contributions relies on precise determinations of the proton form factors at low  $Q^2$ , including the impact of two-photon exchange corrections [31] (discussed further below).

While the form factors encode information on the spatial structure of the proton, there are theoretical issues in extracting the spatial charge and magnetization distributions, discussed in detail elsewhere [32–36]. However, the difficulty in extracting true rest-frame distributions for the proton does not interfere with the comparison of form factor measurements and proton size/structure corrections to atomic levels in hydrogen. Extractions of the proton charge radius [37–41] define the proton root-mean-square (RMS) radius as the slope of the form factor at  $Q^2 = 0$ . This definition is consistent with the RMS radius needed in Lamb shift measurements in hydrogen [42] and muonic hydrogen [43]. Corrections to the hyperfine splitting [44–46] are also extracted directly from the form factors. The charge radius is of particular interest at present, due to the conflicting results between Lamb shift measurements on muonic hydrogen [43] and the electron scattering results and measurements from the Lamb shift in electronic hydrogen [42].

This experiment was motivated by the ideas discussed above: mapping out the large scale proton structure, the benefit of improved precision in proton form factors in order to extract strange quark form factors (and ultimately the proton weak radius) from parity violating measurements, and the importance of reducing the uncertainty in hyperfine splitting calculations arising from proton finite-size corrections.

## II. PREVIOUS MEASUREMENTS

Since the 1960s, measurements of the unpolarized cross section for elastic e–p scattering have been used to separate  $G_E$  and  $G_M$ . The cross section is proportional to  $(\tau G_M^2 + \varepsilon G_E^2)$ , where  $\tau = Q^2/4m_p^2$ , and  $\varepsilon = (1 + 2(1 + (Q^2/4m_p^2)) \tan^2 \theta/2)^{-1}$ . Keeping  $Q^2$  fixed while varying  $\varepsilon$  allows for a “Rosenbluth separation” [47] of the contributions from  $G_E$  and  $G_M$ . At high  $Q^2$ , the factor of  $\tau G_M^2$  dominates, as  $\tau$  becomes large and  $G_M^2 \gg G_E^2$  (with  $G_M/G_E = \mu_p$  at  $Q^2 = 0$ ). This makes extraction of  $G_E$  difficult, as it contributes only a small, angle-dependent correction to the larger cross section contribution from  $G_M$ . Similarly, in the limit of very small  $Q^2$ , and thus very small  $\tau$ , it is difficult to isolate  $G_M$  except in the limit where  $\varepsilon \rightarrow 0$ , i.e. scattering angle  $\rightarrow 180^\circ$ .

Polarization measurements are sensitive to the *ratio*  $G_E/G_M$  and thus, when combined with cross section measurements, can cleanly separate the electric and magnetic form factors, no matter how small their contribution to the cross section becomes. It has been known for some time [2–5] that measurements of polarization observables would provide a powerful alternative to Rosenbluth separation measurements, but only in the last

decade or so have the high polarization, high intensity electron beams been available, combined with polarized nucleon targets or high efficiency nucleon recoil polarimeters [19–21].

The first such measurements for the proton [6, 7] showed a decrease in  $\mu_p G_E/G_M$  with  $Q^2$ , which differed from the existing Rosenbluth separation measurements, which showed approximate form factor scaling, i.e.  $\mu_p G_E/G_M \approx 1$ . This discrepancy appeared to be larger than could be explained even accounting for the scatter in the previous Rosenbluth measurements [11]. A measurement using a modified Rosenbluth extraction technique [48] was able to extract the ratio  $\mu_p G_E/G_M$  with precision comparable to the polarization measurements, and showed a clear discrepancy, well outside of the experimental systematics for either technique. Experiments extending polarization measurements to higher  $Q^2$  show a continued decrease of  $\mu_p G_E/G_M$  with  $Q^2$  [7, 9, 10].

It was suggested that the two-photon exchange (TPE) correction may be able to explain the discrepancy between the two techniques [12, 16]. While these corrections are expected to be of order  $\alpha_{EM} \approx 1\%$ , they can have a similar  $\varepsilon$  dependence to the contribution from  $G_E$ . Because the contribution to  $G_E$  is small at large  $Q^2$ , a TPE correction of a few percent could still be significant in the extraction of  $G_E$ . It was estimated that a TPE contribution of  $\sim 5\%$ , with a linear  $\varepsilon$  dependence, could explain the difference [12, 49], and early calculations suggested effects of a few percent, with just such a linear  $\varepsilon$ -dependence [16, 50]. These corrections should also modify the polarized cross section measurements, but it should be a percent-level correction in the extraction of  $G_E/G_M$ , as there is no equivalent amplification of the effect. Including the best hadronic calculations available yields consistency between the two techniques, and good separation of  $G_E$  and  $G_M$  up to high  $Q^2$  [13, 15]. Comparisons of electron–proton and positron–proton scattering can be used to isolate TPE contributions [51], and a series of such measurements are currently planned or underway [52–54].

At low  $Q^2$  values, the TPE should be well described by the hadronic calculations [13, 55], and in fact the contributions are small for  $0.3 < Q^2 < 0.7$  GeV<sup>2</sup>. While this is a region where high precision Rosenbluth separations are possible, measurements prior to 2010 had relatively large uncertainties, typically 3–5% or more on  $\mu_p G_E/G_M$ . Measurements using polarization observables in this region can provide a significant improvement in precision, even in this low  $Q^2$  regime. The MIT-Bates BLAST experiment made measurements of  $\mu_p G_E/G_M$  using a polarized target [56] for  $0.15 < Q^2 < 0.6$  GeV<sup>2</sup>, with typical uncertainties around 2%, about a factor of two improvement over most earlier data. The experiment, which provided the best knowledge of the low  $Q^2$  proton form factor ratio when published, measured values below unity for  $Q^2 > 0.2$  GeV<sup>2</sup>, but concluded that the overall results were consistent with unity over the range

of the experiment. Combined with the high- $Q^2$  JLab data, which showed a clear deviation of  $\mu_p G_E/G_M$  for  $Q^2 \gtrsim 0.8$  GeV<sup>2</sup>, this suggested that the ratio was unity at very low  $Q^2$  and then began to fall somewhere in the range of 0.2–0.7 GeV<sup>2</sup>. The fact that there was no clear indication of where the ratio began to fall below unity was one of the motivating factors for this measurement. The updated results of this reanalysis of [1] provide an independent extraction of  $\mu_p G_E/G_M$  in this kinematic region, with precision comparable to the BLAST results. More recently, JLab experiment E08-007 [41], a high-statistics follow up to the work we present here, used the same polarization transfer techniques but with coincident detection of the final-state electron and proton for all kinematics, yielding measurements of  $\mu_p G_E/G_M$  with average uncertainties below 1.2%.

Last year, new measurements in this  $Q^2$  region were also obtained by an experiment at Mainz [40]. The experiment made high-precision measurements of unpolarized cross sections at  $\sim 1400$  kinematic points for  $Q^2 < 1$  GeV<sup>2</sup>. While they do not provide direct Rosenbluth extractions of  $G_E$  and  $G_M$ , they show a global fit to their cross section results. Their extraction of  $G_M$  is systematically 2–4% above previous world’s data, implying a difference of 4–8% in the extrapolation of the cross section to  $\varepsilon = 0$ . It is difficult to determine how much of their error band could be strongly correlated in  $Q^2$ , as there is no information given on the size or sources of systematic uncertainty assumed in their analysis. While they apply a very limited form of the two-photon exchange corrections [57], which is neglected in most previous extractions, this should only reduce their value of  $G_M$  relative to the uncorrected results, implying that the true discrepancy is even larger. At this point, it is not clear why there is such a large discrepancy between their fit and previous measurements.

### III. EXPERIMENT DETAILS

This experiment was carried out in Hall A of the Thomas Jefferson National Accelerator Facility (JLab), in the summer and fall of 2006, as part of experiment E05-103 [58]. While the experiment was focused on polarization observables in low energy deuteron photodisintegration [59], elastic electron–proton scattering measurements used to calibrate the focal plane polarimeter provided high statistics data that allowed for an improved extraction of the proton form factor ratio  $\mu_p G_E/G_M$  at low  $Q^2$ .

A polarized electron beam was incident on a cryogenic liquid hydrogen target, nominally 10 cm in length for the 362 MeV beam energy running and 15 cm for the 687 MeV settings (the target length was misstated as 15 cm for all runs in the previous publication [1]). The target cells are Al, with beam entrance windows about 0.1 mm thick, and beam exit and sides  $\sim 0.2$  mm thick (with some variation between the different targets). Elas-

tic e-p scattering events were identified by detecting the struck proton in one of the High Resolution Spectrometers (HRS) [60]. Data were taken with a longitudinal polarization of approximately 40% and with the beam helicity flipped pseudo-randomly at 30Hz. For some settings, the scattered electron was detected in the other HRS spectrometer.

The polarization of the struck protons is measured in a focal plane polarimeter (FPP) in the proton spectrometer. Operation and analysis of events in the FPP is described in detail in Refs. [8, 60]. Analysis of the angular distribution of rescattering in the polarimeter allows us to extract the transverse polarization at the detector, which can be used to reconstruct the longitudinal and transverse (in-plane) components of the polarization of the elastically scattered protons. In the Born approximation, the ratio of these polarization components is directly related to the ratio  $G_E/G_M$ ,

$$R \equiv \frac{G_E}{G_M} = -\frac{E_0 + E'}{2m_p} \tan\left(\frac{\theta_e}{2}\right) \frac{C_x}{C_z}, \quad (1)$$

where  $C_{z,x}$  are the longitudinal and transverse components of the proton polarization,  $E_0$  is the beam energy, and  $\theta_e$  and  $E'$  are the scattered electron's angle and momentum (reconstructed from the measured proton kinematics). Because the extraction of  $\mu_p G_E/G_M$  depends on the ratio of two polarization components, knowledge of the absolute beam polarization and FPP analyzing power are not necessary, although high polarization and analyzing power improve the figure of merit of the measurement.

In the experiment, we measure the polarization not at the target, but in the spectrometer focal plane, and the asymmetry in the rescattering is sensitive only to polarization components perpendicular to the proton direction. If we look at the central proton trajectory, where the spectrometer is well represented by a simple dipole, then the transverse component,  $C_x$ , will be unchanged, while the longitudinal component,  $C_z$ , will be precessed in the dipole field. If we chose a spin precession angle,  $\chi$ , near 90 degrees, the longitudinal and transverse polarization components at the target will yield "vertical" and "horizontal" components in the frame of the focal plane polarimeter, allowing for both to be extracted by a measurement of the azimuthal distribution of rescattering in the carbon analyzer. In the analysis, we use a detailed model of the spectrometer to perform the full spin precession, rather than taking a dipole approximation, as described in detail in Ref. [8].

A follow-up experiment, JLab E08-007 [61] was proposed to make extremely high precision measurements in this kinematic regime. The measurement was run in the summer of 2008, and in the analysis of the E08-007 data, it was observed that the result was somewhat sensitive to the cuts applied to the proton kinematics when isolating elastic e-p scattering.

In this experiment, only the proton was detected for most kinematic settings, and the elastic scattering events

TABLE I: Kinematics and FPP parameters for the measurements.  $\theta_{lab}^p$  and  $T_p$  are the proton lab angle and proton kinetic energy, respectively.  $T_{analyzer}$  is the thickness of the FPP carbon analyzer and  $\chi$  is the spin precession angle for the central trajectory. The final column shows which kinematics had single-arm (S), coincidence (C), or a combination of both (C/S).

$Q^2$ (GeV <sup>2</sup> )	$E_e$ (GeV)	$\theta_{lab}^p$ (deg)	$T_p$ (GeV)	$T_{analyzer}$ (inches)	$\chi$ (deg)	S/C
0.215	0.362	28.3	0.120	0.75	91.0	S
0.235	0.362	23.9	0.130	0.75	91.9	S
0.251	0.362	18.8	0.140	0.75	92.7	S
0.265	0.362	14.1	0.148	0.75	93.4	S
0.308	0.687	47.0	0.170	2.25	95.3	C
0.346	0.687	44.2	0.190	3.75	97.0	C&S
0.400	0.687	40.0	0.220	3.75	99.6	S
0.474	0.687	34.4	0.260	3.75	103.0	S

were isolated using cuts on the over-determined elastic kinematics. In the original analysis [1], relatively loose cuts were applied because the measurement was statistics limited and little cut dependence had been observed in previous measurements [7, 8, 62]. Most of these measurements had high resolution reconstruction of both the proton and electron kinematics, and so loose cuts on the combined proton and electron kinematics provided clean isolation of the elastic peak. In addition, the previous measurements were generally at higher  $Q^2$  and so of significantly lower statistical precision, typically 3-5%, so it was difficult to make precise evaluation of the impact of tight cuts on the proton kinematics. Because the elastic events could be cleanly identified without tight cuts on the proton kinematics, this was not considered to be a significant concern.

In the follow-up experiment, E08-007 [61], the electron was detected in a large acceptance spectrometer with limited momentum and angle resolution. The electron detection led to significant suppression of scattering from the target windows, but the poor electron resolution required that the elastic peak be defined using cuts on the proton kinematics. Because of this, and the high statistics of the data set, it was possible to make detailed studies of the cut dependence of the result. It was found that there were small but noticeable changes in the extracted form factor ratio if the proton kinematic cuts were made too loose, even in cases where the endcap contributions were small.

Motivated by these issues, we reanalyzed the data from our experiment. We include a more careful examination of cuts used to identify the proton events and an updated evaluation of the contribution from the target endcaps. With our new, more restrictive cuts, there were small but systematic changes in the extracted form factors. These were mainly due to the reduction in the contribution from electron scattering in the Aluminum endcaps rather than

any changes in the events corresponding to scattering from hydrogen.

One of the most important issues in the original analysis was the correction for events that came from scattering in the Aluminum endcaps of the targets, and there were several difficulties involved in making these corrections. For systematic checks, we took data with the elastic peak centered on the focal plane, but also with the spectrometer momentum approximately 2% higher and lower, to map out the response of the FPP across the focal plane. Data on the Aluminum dummy targets were typically taken for only one setting, and so there was a systematic uncertainty associated with the stability of the size of the background contamination and the possible variation of the polarization transfer coefficients measured from the dummy target. Data were taken using both 15 cm and 10 cm cryogenic hydrogen targets, but only dummy foils for the standard 4 cm and 15 cm cryotargets were available, yielding some additional systematic uncertainties for the 10 cm targets. Finally, for some runs the beam position was not perfectly stabilized on the dummy foils and the beam, rastered to a 4 by 4 mm<sup>2</sup> spot at the target, either partially missed the dummy foils or impinged on both the 4 cm and 15 cm dummy targets. While the beam position is continuously monitored and we correct for any deviation in the event reconstruction based on the position, the luminosity is not well known if the beam is partially missing the foils. Therefore, the relative normalization of the contribution from the target endcaps and the dummy foils had to be determined by looking at quasielastic events that are above the threshold for scattering from the proton, rather than being calculated directly, yielding an additional systematic in the relative normalization of the endcaps and dummy foils.

In the original analysis, endcap scattering typically yielded 3–5% of the cross section after all cuts were applied (much less for the two coincidence settings), so there was a small but significant correction. Because of the issues mentioned above, there were very large systematic uncertainties associated with these corrections. In addition, the original analysis applied the full set of cuts for elastic scattering to data from the dummy target, yielding measurements of the polarization coefficient for endcap scattering with extremely poor statistics and thus large fluctuations. We now use much tighter cuts on the reconstructed target position to try to remove most of the endcap contributions, resulting in contributions of  $\lesssim 0.5\%$ . While the cuts reduce the statistics of the main measurement somewhat, the final uncertainty is often better, as the endcap subtraction, which had large statistical and systematic uncertainties, is now much smaller. We also use looser cuts when extracting  $C_x$  and  $C_z$  from scattering in the aluminum endcaps, with an extra systematic uncertainty applied to account for possible cut dependence.

#### IV. ANALYSIS DETAILS

For elastic scattering using an electron beam with a known energy the complete scattering kinematics can be determined from the measurement of a single kinematic quantity, typically the angle or energy of the final state electron or proton. If two quantities are measured, then the consistency of the two kinematic variables can be used to determine if the event was associated with elastic scattering. For this analysis, we use the proton scattering angle and momentum to reconstruct the kinematics and to identify elastic events. For some kinematics, the electron was also detected, which allows for almost complete suppression of events coming from quasielastic scattering in the aluminum entrance and exit windows of the target. To identify the elastic peak, we use the difference between the measured proton momentum and the momentum calculated based on the measured proton angle measured proton angle. The specific variable we use is  $DpKin$ , which is the momentum difference,  $p_p - p_{elastic}(\theta_p)$ , divided by the central momentum setting of the proton spectrometer. This yields a fractional momentum deviation from the expectation for elastic scattering.

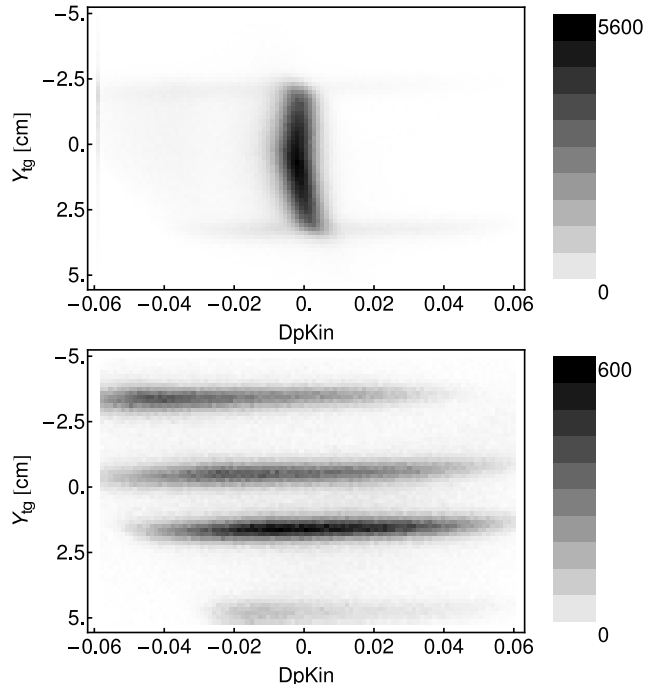


FIG. 1: Reconstructed target position  $Y_{tg}$  vs.  $DpKin = (p_p - p_{elastic}(\theta_p))/p_{HRS}$  for the measurements on the 10 cm liquid hydrogen target (top) and on the 4 cm and 15 cm Aluminum “dummy” foils (bottom). Note that  $Y_{tg}$  is the position transverse to the spectrometer optic axis, not the position along the beamline; this difference leads to the target dimensions being reduced by a factor of  $\approx 2$  here. The elastic peak is clearly visible at  $DpKin \approx 0$  for the LH2 target, while the broad quasielastic contributions from endcap scattering are visible at the ends of the LH2 target.

Figure 1 shows the distribution of events versus  $DpKin$  and the reconstructed target position,  $Y_{tg}$ , as seen by the spectrometer. For the hydrogen target (top panel), there is a strong peak at  $DpKin \approx 0$ , corresponding to elastic events. At the extreme  $Y_{tg}$  values, there is a faint but broad distribution corresponding to quasielastic scattering in the endcaps. We apply a cut to  $Y_{tg}$  to remove most of the contribution from the endcap scattering, and use the measurements from the 4 cm and 15 cm dummy target (bottom panel) to subtract the residual contribution. Note that for the spectra shown in Fig. 1, the length of the LH2 target does not match either the inner or the outer pair of foils from the dummy target. This means that the acceptance as a function of  $DpKin$  depends on  $Y_{tg}$  and so will not be identical for the endcaps and the foils in the dummy target. This is clear for the outer foils of the dummy target, where there is a significant loss of events at extreme positive (negative) values of  $DpKin$  for the upstream (downstream) dummy foils.

For each  $Q^2$  setting, three measurements were taken; one with the elastic peak positioned at the central momentum of the spectrometer, and two where the elastic peak was shifted up (down) by 2% in momentum. This allowed us to verify that the result was independent of the position of the events on the focal plane. However, dummy events were typically taken at only one of these three settings, and the extracted endcap contribution and quasielastic recoil polarizations taken from that measurement were applied to all three settings, so the  $DpKin$  distributions will not be exactly identical, especially far away from the elastic peak. The dummy spectra are normalized to match the observed “super-elastic” contribution ( $DpKin > 0.03$  in Fig. 2) in the LH2 data, using only the inner foils for the dummy target, as they have a  $DpKin$  acceptance which better matches the endcaps. Figure 2 shows the spectra for the LH2 target (thick black histogram) and the dummy target (grey histogram), after the dummy target has been normalized in the region indicated by the vertical dashed lines. After normalizing the spectra in this region, we can determine the endcap contribution under the elastic peak. The region used to define elastic events in the analysis is indicated by the vertical dotted lines. We take a conservative approach and apply a 50% systematic uncertainty to the size of the endcap contribution when making the correction for these events to account for the impact of the different  $DpKin$  spectra between the endcaps and the dummy foils and possible variation for the settings which are shifted by  $\pm 2\%$  in momentum.

Having determined the contribution from endcap scattering, we use the data from the dummy targets to determine the contributions from quasielastic scattering to the recoil polarization components  $C_x$  and  $C_z$ . If we apply the same cuts to the dummy target as we use in the analysis of the hydrogen, there is very little data left, and we can not make a reliable extraction of  $C_x$  and  $C_z$ . For the quasielastic scattering, we use all four aluminum foils and a broader cut on  $DpKin$  to determine the quasielas-

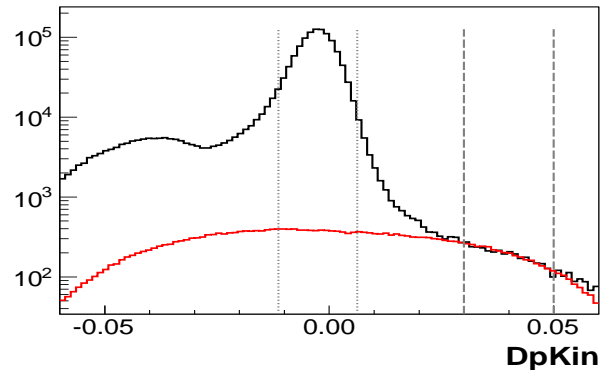


FIG. 2: (Color online) The  $DpKin$  distribution for the hydrogen target (thick black histogram) and the dummy targets (thin red histogram). The dashed vertical lines indicate the region used to normalize the dummy contribution to match the contribution from the aluminum endcaps of the hydrogen target and the vertical dotted lines indicate the part of the elastic peak used in the analysis.

tic values for  $C_x$  and  $C_z$ , and then assume that the coefficients are identical when looking at the central part of the quasielastic spectrum. Comparisons showed complete consistency between the extracted values of  $C_x$  and  $C_z$  when comparing the inner and outer dummy foils for all kinematics, or when comparing the central part of the quasielastic peak to the off-peak contributions. Because we could not make a precise determination of  $C_x$  and  $C_z$  without averaging over a larger kinematic region, we apply an uncertainty to  $C_x$  and  $C_z$  of 0.02 and 0.05 respectively, compared to typical values for these polarization components in this experiment of 0.08–0.2 for  $C_x$  and 0.15–0.3 for  $C_z$ .

In the original analysis [1], the  $Y_{tg}$  cut was loose and so there was a large (3–5%) contribution from endcap scattering which had to be subtracted. Because the tight cuts used on the elastic events were also applied to the dummy spectra used to subtract endcap scattering contributions, the statistical uncertainty on these subtractions could be very large. Therefore, fluctuations in the low statistics dummy measurements led to large uncertainties and significant fluctuations in the dummy-subtracted measurements. In the present analysis, the endcap contributions are greatly reduced, with a maximum contribution well below 1%, such that the conservative systematic uncertainties assumed for the dummy normalization and polarization coefficients yield only small uncertainties in the final result. While the tighter cuts yield slightly reduced statistics in the elastic peak, the total statistical uncertainty is sometimes smaller because the background contribution was reduced. Note that for a few settings, additional runs were included, improving the statistics by 5–15%, but this was a small effect compared to the modified cuts.

There were also some small changes in the evaluation

of the systematic uncertainties. In the previous analysis, the systematic uncertainty from the endcap contribution was folded into the reported statistical uncertainties, and these are now part of the quoted systematics. In addition, the estimated systematics are somewhat larger than in the previous analysis, due to a more detailed analysis of the uncertainty in the spin precession through the spectrometer [63].

The proton energy loss, which can be significant for the low  $Q^2$  kinematics, was also more carefully evaluated, leading to a small change in the average  $Q^2$  for each bin. For the 362 MeV running, where the proton was detected at small angles, the energy loss depends on the position in the target where the scattering occurs. Figure 3 shows  $DpKin$  vs.  $Y_{tg}$  for one of the 362 MeV runs with an average proton energy loss is applied to all events. Positive  $Y_{tg}$  values correspond to the upstream portion of the target, where all events exit through the side of the target and travel through a constant amount of hydrogen and aluminum and can be well corrected assuming a fixed energy loss. Events that exit through the downstream end of the target lose less energy because they pass through less material, yielding a  $Y_{tg}$ -dependent energy loss, and thus a higher apparent proton momentum, for events that occur near the exit window. For the kinematics where this effect is important, we apply a  $Y_{tg}$ -dependent cut, cut corresponding to a two-sigma region around the elastic peak for each region of  $Y_{tg}$ , as indicated by the graphical cut displayed in Fig. 3. The reconstructed value of  $DpKin$  is only used to select elastic events, so while a position-dependent energy loss could have been applied, one would still end up with the same set of good events passing the cuts. In our approach, we are not sensitive to any imperfections in the energy loss correction, since we use a two-sigma cut for all  $Y_{tg}$  values.

TABLE II: Kinematic-dependent cuts applied to the data. The  $Y_{tg}$  cut is chosen to significantly suppress any contributions from the target endcap (as shown in Fig. 3).

$Q^2$ (GeV <sup>2</sup> )	$\theta_{lab}^p$ (deg)	$Y_{tg}$ cut (cm)	$\delta p/p$ cut
0.215	28.3	$-0.022 < Y_{tg} < 0.018$	$ \delta p/p  < 0.045$
0.235	23.9	$-0.022 < Y_{tg} < 0.018$	$ \delta p/p  < 0.045$
0.251	18.8	$-0.018 < Y_{tg} < 0.012$	$ \delta p/p  < 0.045$
0.265	14.1	$-0.014 < Y_{tg} < 0.010$	$ \delta p/p  < 0.045$
0.308	47.0	$-0.025 < Y_{tg} < 0.020$	$ \delta p/p  < 0.040$
0.346	44.2	$-0.025 < Y_{tg} < 0.020$	$ \delta p/p  < 0.040$
0.400	40.0	$-0.028 < Y_{tg} < 0.022$	$ \delta p/p  < 0.040$
0.474	34.4	$-0.024 < Y_{tg} < 0.020$	$ \delta p/p  < 0.040$

The kinematic-dependent cuts are detailed in Table II. In addition, several cuts were applied to all kinematics. A cut was applied on the out-of-plane angle,  $|\theta_{tg}| < 0.06$  rad, and the in-plane angle,  $|\phi_{tg}| < 0.03$  rad, to ensure events were inside of the angular acceptance of

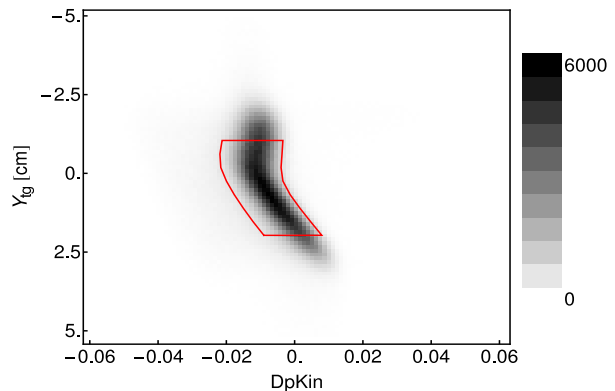


FIG. 3: (Color online) The reconstructed target position,  $Y_{tg}$  vs.  $DpKin$ , the deviation of the momentum from the expected elastic peak position. A correction for the average energy loss is applied, but there is a significant difference for events on the upstream side of the target, which exit through the side wall of the target, and events which occur nearer the downstream end of the target and have less energy loss. The band indicates the graphical cut placed on these runs, to approximate a two-sigma range for each  $Y_{tg}$  value.

the spectrometer. A two-sigma cut was applied on the  $DpKin$  peak, with a  $Y_{tg}$ -dependence cut for the low energy kinematics to account for the position-dependent average energy loss as shown in Figure 3. The tracks before and after the Carbon analyzer were used to determine the scattering location and scattering angle in the analyzer. Events were required to have the secondary scattering occur within the analyzer, and angle between 5 and 50° were accepted. In addition, we apply a cone test [8] to ensure that there is complete azimuthal acceptance in the FPP. We do this by requiring that the FPP would have accepted events with any azimuthal angle given the reconstructed vertex and scattering angle. This ensures that any asymmetry in the acceptance or distribution of events does not lead to a difference in the scattering angle distribution for vertical and horizontal rescattering. A significant difference between the rescattering distribution for vertical and horizontal rescattering events would yield a different average analyzing power, and the analyzing power would not cancel out in the ratio of polarization components.

The combination of the more restrictive cuts on the elastic events and the associated reduction in contamination due to scattering from the target windows leads to a reduction in the extracted ratio that is typically at the 1–2% level. The largest effect is due to the improved correction for endcap scattering, mainly due to cuts which significantly reduced the size of this contribution. There is also a 1% reduction in the coincidence settings, where there are negligible endcap contributions, which is due to the tighter cuts on the proton kinematics. Tight elastic kinematics cuts using just the proton will remove events where there is a larger than average

TABLE III: Systematic uncertainties on  $R = \mu_p G_E/G_M$ . See text for details.

$Q^2$ (GeV <sup>2</sup> )	$\delta R$ (endcap)	$\delta R$ (optics)	$\delta R$ (cuts)
0.215	0.0012	0.0079	0.0141
0.235	0.0004	0.0079	0.0120
0.251	0.0003	0.0078	0.0107
0.265	0.0003	0.0076	0.0098
0.308	–	0.0091	0.0077
0.346	–	0.0086	0.0066
0.400	0.0010	0.0088	0.0056
0.474	0.0007	0.0117	0.0049

error in the reconstruction of the proton scattering angle or momentum due to multiple scattering or imperfect track reconstruction. While these errors are small, the reconstructed kinematics are used to determine the spin propagation through the spectrometer, and thus the impact of the poor reconstruction may be amplified in evaluating the spin precession. Table III shows the various contributions to the systematic uncertainty as a function of  $Q^2$ . At high  $Q^2$ , the uncertainty in the spin precession due to imperfect knowledge of the spectrometer optics dominates. At low  $Q^2$ , the uncertainty is dominated by our ability to determine the cut dependence of the result. The cut-dependent uncertainties come mainly from two sources; possible variation of the result due to the cuts on  $y_{tg}$  and  $DpKin$ . While no systematic cut dependence with the  $y_{tg}$  cut was observed, we apply a 0.4% uncertainty as a conservative estimate based on examining the variation of  $\mu_p G_E/G_M$  with the  $y_{tg}$  cut, in particular for the coincidence data where the background contributions are smaller. For  $DpKin$ , we estimate the uncertainty based on varying the width of the cut around the elastic peak. This was done for both these data and the E08-007 results and no systematic cut dependence was observed, so the scatter of the results was taken as a conservative estimate of the systematic uncertainties. Because the data taken at low beam energy do not have sufficient statistics to set precise limits, we fit the uncertainties from the higher energy measurements and the E08-007 results and find a behavior consistent with  $1/Q^4$ , which we use to obtain the quoted uncertainties for the low  $Q^2$  values.

## V. RESULTS

The results of the reanalysis are given in Table IV and shown in Figure 4, which presents the updated results along with previous measurements and a selection of fits. The updated analysis yielded a systematic decrease of  $\sim 1\%$  in the extracted ratio, except for the highest  $Q^2$  point which decreased by 5%. The analyzing power has been extracted from these data [64], but the quality of

this extraction does not impact these results, as the analyzing power cancels out in the ratio of Eq. 1. However, because the FPP efficiency and analyzing power are significantly lower for the data taken at a beam energy of 362 MeV (due to the lower proton momentum and thinner analyzer), the statistical uncertainty in these points is much larger. The two-photon exchange corrections from the hadronic calculation of Blunden, et al. [55] are 0.35% for the data below  $Q^2 = 0.3$  GeV<sup>2</sup> and 0.2% for the higher  $Q^2$  points. This is well below the statistical and systematic uncertainties for all points, and no correction (or uncertainty) for the TPE effects is included in the extraction.

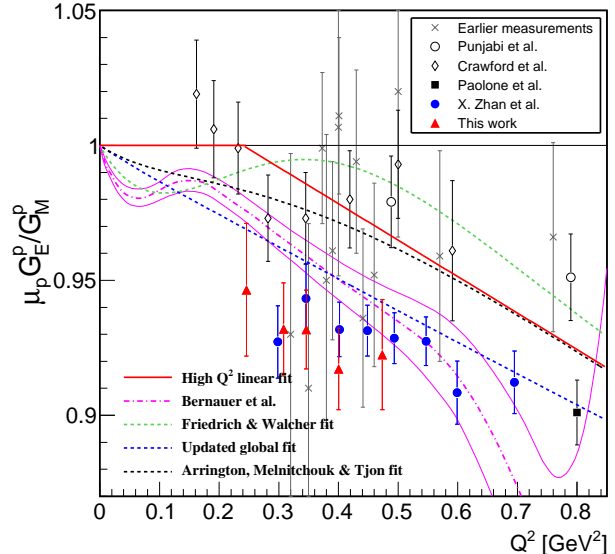


FIG. 4: (Color online) The proton form factor ratio as a function of  $Q^2$  (with the four low- $Q^2$  measurements combined into one data point) shown with previous extractions with total uncertainties  $\leq 3\%$ . The curves are various fits [7, 13, 26, 41], while the dot-dashed curve and associated error bands show the result of the fit to the recent Mainz measurements [40].

The results in Fig. 4 show that the original conclusions of [1] are largely unaffected. The new results support even more clearly the conclusion that the ratio  $\mu_p G_E/G_M$  is below one even for these low  $Q^2$  values, with the change from previous Rosenbluth separations being driven mainly by a change in  $G_E$ , with a smaller change in  $G_M$ . The previous hint of a local minimum near  $Q^2 = 0.35 - 0.4$  GeV<sup>2</sup> was a consequence of the point near 0.5 GeV<sup>2</sup>, and there is no longer any indication for this in our measurement. These results further support the observation that the decrease of the ratio below unity occurs at low  $Q^2$ , and thus we expect that there will be a slightly larger impact on the extraction of strange quark contributions, as discussed in the original paper [1].

A comparison of the high-precision measurements at low- $Q^2$  shows some small but systematic differences. The

TABLE IV: Experimental Results.  $R$  is given along with its statistical and systematic uncertainties. The last column (f) is the fractional contribution from scattering in the target end-caps, along with the statistical uncertainty; a 50% systematic uncertainty is also applied. The contribution is negligible for the coincidence settings. For  $Q^2 = 0.474 \text{ GeV}^2$ , dummy measurements were taken at all three sub-settings, and the range of results is given. <sup>†</sup>The final entry is the average of the four low-statistics point below  $Q^2 = 0.3 \text{ GeV}^2$ .

$Q^2$ ( $\text{GeV}^2$ )	$R = \mu_p G_E/G_M$	f (%)
0.215	$0.8250 \pm 0.0483 \pm 0.0162$	0.26(3)
0.235	$0.9433 \pm 0.0414 \pm 0.0144$	0.13(2)
0.251	$0.9882 \pm 0.0420 \pm 0.0132$	0.19(3)
0.265	$0.9833 \pm 0.0349 \pm 0.0124$	0.16(2)
0.308	$0.9320 \pm 0.0123 \pm 0.0119$	–
0.346	$0.9318 \pm 0.0098 \pm 0.0108$	–/0.40(2)
0.400	$0.9172 \pm 0.0109 \pm 0.0105$	0.65(4)
0.474	$0.9225 \pm 0.0160 \pm 0.0127$	0.4–0.6
0.246 <sup>†</sup>	$0.9465 \pm 0.0204 \pm 0.0137$	n/a

results from the Mainz cross section measurements [40] are 1–2% above the recoil polarization measurements from this work and the lower  $Q^2$  results from the recent JLab E08-007 measurement [41], although they are in agreement with the E08-007 results at higher  $Q^2$  values. One concern for the results extracted from the Mainz cross section measurements is the sensitivity to two-photon exchange (TPE) corrections [15]. For the kinematics of the Mainz experiment, these corrections are fairly small,  $\lesssim 2\%$ , but this is very large compared to the statistical ( $\lesssim 0.2\%$ ) and systematic ( $\lesssim 0.5\%$ ) uncertainties applied in the global fit to  $G_E$  and  $G_M$ . Thus, if ignored, this could yield significant corrections compared to the quoted uncertainties. Coulomb corrections were applied using the prescription of McKinley and Feshbach [57], which corresponds to the  $Q^2 = 0$  limit of the Coulomb distortion correction (the soft-photon approximation of the full TPE corrections). However, over much of the  $Q^2$  range of the experiment, applying the  $Q^2 = 0$  correction is worse than neglecting the correction altogether, as the Coulomb correction changes sign at  $Q^2 \approx 0.15 \text{ GeV}^2$  [65]. An estimate of the impact of these corrections [66] suggests that an improved prescription would decrease  $\mu_p G_E/G_M$  extracted from the cross sections by 1–3% for  $Q^2 \gtrsim 0.1 \text{ GeV}^2$  in a direct Rosenbluth separation, although a more complete analysis is required to determine the impact on their global fit. Bernauer *et al.*, have examined the impact of these corrections [67] in more detail, although the TPE prescription they apply [68] is only valid up to  $Q^2 = 0.1 \text{ GeV}^2$ . They find that their extracted value for  $\mu_p G_E/G_M$  changes by more than the total quoted uncertainty for all  $Q^2$  values up to  $0.1 \text{ GeV}^2$ , and while they find smaller changes at larger  $Q^2$  values, this is where the prescription is not expected

to be valid.

If the Coulomb corrections bring the Rosenbluth [40] extractions into agreement with the recoil polarization data, there is still a small systematic disagreement between these and the polarized target measurements from BLAST [56]. At this point, we are unaware of any theoretical argument that would explain a difference between the results of the two different polarization techniques. This discrepancy can be further examined in the second phase of the JLab E08-007 experiment [61] which will make extremely high precision measurements of  $\mu_p G_E/G_M$  down to  $Q^2 \approx 0.015 \text{ GeV}^2$ , allowing for a comparison with the BLAST measurements using the same basic technique.

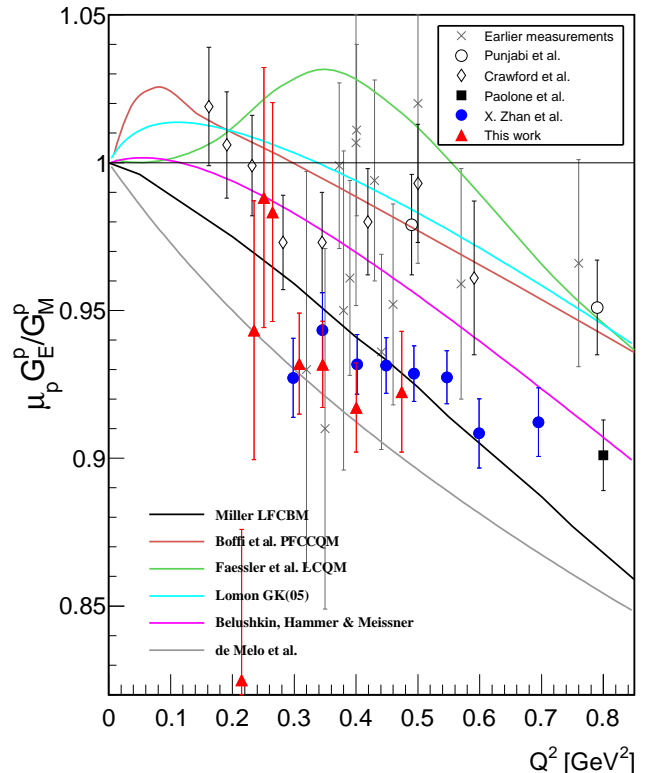


FIG. 5: (Color online) The proton form factor ratio  $\mu_p G_E/G_M$  vs.  $Q^2$ , compared to several low- $Q^2$  models. The curves shown are Miller’s light-front cloudy-bag model calculation [69]; Boffi’s point-form chiral constituent quark model calculation [70]; Faessler’s light-front quark model calculation [71]; Lomon’s vector-meson dominance model [72]; the dispersion analysis of Belushkin, Hammer and Meissner [73]; and the model of de Melo *et al.* [74].

Figure 5 shows the measurements compared to a set of theoretical curves. The first type of calculation is based on the constituent quark models, which was quite successful in describing the ground state baryon static properties. To calculate the form factors, relativistic effects need to be considered. Miller [69] performed a calculation in the light-front dynamics including the effect from

the pion cloud. Boffi *et al.* [70] performed a point form calculation in the Goldstone boson exchange model with point-like constituent quarks. Faessler *et al.* [71] used a chiral quark model where pions are included perturbatively and dress the bare constituent quarks by mesons in a Lorentz covariant fashion. Another group of calculations is based on the Vector Meson Dominance (VMD) picture, in which the scattering amplitude is written as an intrinsic form factor of a bare nucleon multiplied by an amplitude derived from the interaction between the virtual photon and a vector meson. This type of models usually involve a number of free parameters for the meson mass and coupling strength. Lomon [72, 75, 76] performed the VMD fits by including additional vector mesons and pQCD constraints at large  $Q^2$ . Belushkin *et al.* [73] performed a calculation using dispersion relation analysis with additional contribution from  $\rho\pi$  and  $K\bar{K}$  continua. More recently, de Melo *et al.* [74] performed a calculation in the light-front VMD model by considering the non-valence contribution of the nucleon state. While most of the theoretical curves are a few percent higher, the calculations of Miller [69] and de Melo *et al.* [74] generally reproduce the large deviation from  $\mu_p G_E/G_M = 1$  in this low  $Q^2$  region, emphasizing the pion cloud or non-valence effect.

Our new results, as well as other high-precision measurements at low  $Q^2$ , show that  $\mu_p G_E/G_M < 1$  even down to very low values of  $Q^2$ . A global fit [41] to the cross section and polarization measurements in this region, including the data presented in this work, indicates that  $G_E$  is  $\sim 2\%$  below previous fits that did not include the low  $Q^2$  polarization measurements, while  $G_M$  is approximately 1% higher. These small changes in the low  $Q^2$  form factors impact other measurements as well. For example, it was recently pointed out [77] that the reduction in the form factor yields an agreement between studies of the asymmetry in the  $D(e,e'p)n$  reaction at low missing momentum in polarized target measurements at NIKHEF and MIT-Bates [78–80], and recent measurements at Jefferson Lab [81]. Similarly, this small shift in  $G_E$  and  $G_M$  at low  $Q^2$  modifies the expected asymmetry in parity-violating elastic electron–proton scattering, which serves as the baseline when extracting the strange-quark contribution to the proton form factors [27–30]. The effect is relatively small for any given extraction, especially at forward angles where there is a partial cancellation due to the changes in  $G_E$  and  $G_M$ . However, because this is a systematic correction to all such measurements, the updated form factors could have a small net contribution on the extracted strange-quark contributions.

The form factors at very low  $Q^2$  are important in both extracting the proton size and as input to other finite-size corrections in atomic physics, e.g. the Zemach radius in hyperfine splitting [44–46]. Measurements of the ratio  $\mu_p G_E/G_M$  are not, by themselves, sufficient to extract the proton radius or calculate the finite-size corrections, as these require the individual form factors  $G_E(Q^2)$  and

$G_M(Q^2)$ . However, the polarization measurements can be used to improve global fits to cross section data, in which determining the relative normalization of different data sets is often the limiting factor in the systematic uncertainties [37]. It is often possible to modify the normalization of certain data sets and modify the ratio  $\mu_p G_E/G_M$  in such a way that the cross section measurements are still relatively well fit. Thus, having direct constraints on  $\mu_p G_E/G_M$  with high precision allows for a better determination of these normalization factors, and an improved extraction of the form factors. The fit of Ref. [13] was updated in Ref. [41] to include the data presented here as well as additional polarization measurements [9, 41, 82], yielding improved extractions of  $G_E$ ,  $G_M$ , as well as the proton charge and magnetization radii. While these polarization measurements do not go as low in  $Q^2$  as one would like for the extraction of the radius, they nonetheless play an important role in the extraction, mainly by providing improved determinations of the relative normalization of the different experiments. In addition, higher order terms in the  $Q^2$  expansion need to be constrained to obtain a measure of the radius [37].

This updated global analysis yielded an RMS charge radius of 0.875(10) fm, consistent with the CODATA value [42] and recent extraction from cross section measurements from Mainz [40]. Combined, these independent extractions based on the electron–proton interaction yield a radius of 0.8772(46) fm [41], more than seven standard deviations from the recently published PSI muonic hydrogen Lamb shift measurement [43] of 0.8418(7) fm. While higher order corrections, which depend on the values of the form factors at finite  $Q^2$ , can modify the extracted radius, these corrections appear to be far too small to explain the discrepancy, although this is still under investigation [83–86]. A recent work [87] has proposed a possible mechanism to explain a difference between electronic and muonic probes of the proton structure, due to off-shell effects in the hadronic intermediate state in the two-photon exchange diagrams. However, while this is an area that has received a great deal of attention in the recent past [83–85, 88–92], the question is still unresolved.

The updated global fit of the low  $Q^2$  data yields a magnetic RMS radius of 0.867(20) fm [41]. This is in reasonable agreement with other extractions, 0.85(3) fm from Kelly [32] and 0.857 from Hammer and Meissner [93]. However, neither of these included Coulomb distortion corrections, and they are global fits that include a large body of high- $Q^2$  data which do not contain useful information on the proton radius, and thus may not be reliable when it comes to examining the radius. Sick [37] extracted the Zemach radius, which depends on both the charge and magnetic distributions, and converting this to a magnetic radius yields a value of 0.855(35) fm [93], in agreement with the updated fit. However, the data used by Sick are also included in this global fit, so these cannot be considered independent extractions. The Mainz result [40] is 0.777(17) fm, well below the other electron

scattering analyses, but the strong  $Q^2$  dependence of the Coulomb distortion at very low  $Q^2$ , neglected in their extraction, may have a significant impact on the extraction of the radius [66]. An updated estimate yields a  $1.5\sigma$  shift in their magnetic radius (and almost no change in the electric radius), yielding  $0.803(17)$  fm [67], where the uncertainty does not include any contribution related to the two-photon exchange corrections. This increased radius is now only  $2.4\sigma$  from our result, but this updated value still appears to be an underestimate, as their weighted averaging of results from different fits [94] leads to a bias towards fits with fewer parameters. They give systematically lower values for the magnetic radius than the fits with more parameters, as one might expect given that the precision of the extraction of  $G_M$  tends to improve as  $Q^2$  increases, and so inclusion of the high- $Q^2$  data can dominate the fit if there is not enough flexibility in the fit. This does not appear to affect their extraction of the charge radius, as the extracted radius does not show the same systematic dependence on the number of fit parameters. This is not surprising, as precise extractions of  $G_E$  are not limited to higher  $Q^2$  values.

Finally, one can use the discrepancy between calculations and measurements of the hyperfine splitting in the hydrogen ground state to extract the magnetic radius, assuming that all of the other proton structure corrections, including the charge radius, are well known. The analysis by Volotka *et al.* [95] yields a radius of  $0.778(29)$  fm, in agreement with the Mainz result [40]. However, an updated calculation [45] which uses updated proton form factors [13] and spin structure is also consistent with the hyperfine splitting even though it takes a larger magnetic RMS radius of  $0.858$  fm, consistent with our results. Thus, it appears that the hyperfine splitting does not have the sensitivity to precisely constrain the magnetic radius, given the current uncertainty in the other portions of the proton structure corrections.

So while the charge radius has a clear discrepancy between muonic hydrogen lamb shift measurements and the

various measurements using the electron–proton interaction, the situation for the magnetic radius is less clear. The extractions of the magnetic radius are more sensitive to small corrections, both for electron scattering and extractions from hyperfine splitting measurements, making it difficult to tell at this point if there are, in fact, real discrepancies between the techniques.

## VI. SUMMARY AND CONCLUSIONS

In summary, we present an updated extraction of the form factor ratio  $\mu_p G_E/G_M$  from the data of Ref. [1]. We find a somewhat lower value for  $\mu_p G_E/G_M$  than the initial extraction for the entire dataset, consistent with two recent high precision measurements [40, 41]. The new analysis does not change our previous conclusion, i.e., that there is clear indication of a ratio smaller than unity, even for low  $Q^2$ , indicating the necessity of including relativistic effects in any calculation of the form factors in this region. Both the form factors and proton charge radius extraction from various e–p scattering measurements are in agreement, and there is still a significant disagreement with the charge radius as extracted from muonic hydrogen [43].

## Acknowledgments

This work was supported by the U.S. Department of Energy, including contract DE-AC02-06CH11357, the U.S. National Science Foundation, the Israel Science Foundation, the Korea Research Foundation, the US-Israeli Bi-National Scientific Foundation, and the Adams Fellowship Program of the Israel Academy of Sciences and Humanities. Jefferson Science Associates operates the Thomas Jefferson National Accelerator Facility under DOE contract DE-AC05-06OR23177.

- 
- [1] G. Ron *et al.*, Phys. Rev. Lett. **99**, 202002 (2007).
  - [2] A. I. Akhiezer, L. N. Rozentsweig, and I. M. Shmuskevich, Sov. Phys. JETP **6**, 588 (1958).
  - [3] A. I. Akhiezer and M. P. Rekalo, Sov. Phys. Dokl. **13**, 572 (1968).
  - [4] N. Dombey, Rev. Mod. Phys. **41**, 236 (1969).
  - [5] R. G. Arnold, C. E. Carlson, and F. Gross, Phys. Rev. C **23**, 363 (1981).
  - [6] M. K. Jones *et al.*, Phys. Rev. Lett. **84**, 1398 (2000).
  - [7] O. Gayou *et al.*, Phys. Rev. Lett. **88**, 092301 (2002).
  - [8] V. Punjabi *et al.*, Phys. Rev. C **71**, 055202 (2005), Erratum-ibid. C **71**, 069902 (2005).
  - [9] A. J. R. Puckett *et al.*, Phys. Rev. Lett. **104**, 242301 (2010).
  - [10] A. J. R. Puckett *et al.* (2011), arXiv:1102.5737.
  - [11] J. Arrington, Phys. Rev. C **68**, 034325 (2003).
  - [12] P. A. M. Guichon and M. Vanderhaeghen, Phys. Rev. Lett. **91**, 142303 (2003).
  - [13] J. Arrington, W. Melnitchouk, and J. A. Tjon, Phys. Rev. **C76**, 035205 (2007).
  - [14] C. E. Carlson and M. Vanderhaeghen, Ann. Rev. Nucl. Part. Sci. **57**, 171 (2007).
  - [15] J. Arrington, P. G. Blunden, and W. Melnitchouk (2011), arXiv:1105.0951.
  - [16] P. G. Blunden, W. Melnitchouk, and J. A. Tjon, Phys. Rev. Lett. **91**, 142304 (2003).
  - [17] J. Arrington, Phys. Rev. C **71**, 015202 (2005).
  - [18] C. E. Hyde-Wright and K. de Jager, Ann. Rev. Nucl. Part. Sci. **54**, 217 (2004).
  - [19] J. Arrington, C. D. Roberts, and J. M. Zanotti, J. Phys. **G34**, S23 (2007).
  - [20] C. F. Perdrisat, V. Punjabi, and M. Vanderhaeghen, Prog. Part. Nucl. Phys. **59**, 694 (2007).
  - [21] J. Arrington, K. de Jager, and C. F. Perdrisat, J. Phys.

- Conf. Ser. **299**, 012002 (2011).
- [22] A. V. Belitsky, X.-d. Ji, and F. Yuan, Phys. Rev. Lett. **91**, 092003 (2003).
- [23] S. J. Brodsky, J. R. Hiller, D. S. Hwang, and V. A. Karmanov, Phys. Rev. D **69**, 076001 (2004).
- [24] J. P. Ralston and P. Jain, Phys. Rev. D **69**, 053008 (2004).
- [25] G. A. Miller, Phys. Rev. C **68**, 022201 (2003).
- [26] J. Friedrich and T. Walcher, Eur. Phys. J. **A17**, 607 (2003).
- [27] D. S. Armstrong et al., Phys. Rev. Lett. **95**, 092001 (2005).
- [28] K. A. Aniol et al., Phys. Lett. B **635**, 275 (2006).
- [29] K. A. Aniol et al., Phys. Rev. Lett. **96**, 022003 (2006).
- [30] A. Acha et al., Phys. Rev. Lett. **98**, 032301 (2007).
- [31] J. Arrington and I. Sick, Phys. Rev. **C76**, 035201 (2007).
- [32] J. J. Kelly, Phys. Rev. C **66**, 065203 (2002).
- [33] G. A. Miller, Phys. Rev. Lett. **99**, 112001 (2007).
- [34] G. A. Miller and J. Arrington, Phys. Rev. **C78**, 032201 (2008).
- [35] G. A. Miller, E. Piasetzky, and G. Ron, Phys. Rev. Lett. **101**, 082002 (2008).
- [36] S. Venkat, J. Arrington, G. A. Miller, and X. Zhan, Phys.Rev. **C83**, 015203 (2011).
- [37] I. Sick, Phys. Lett. B **576**, 62 (2003).
- [38] P. G. Blunden and I. Sick, Phys. Rev. C **72**, 057601 (2005).
- [39] R. J. Hill and G. Paz, Phys. Rev. **D82**, 113005 (2010).
- [40] J. C. Bernauer et al., Phys. Rev. Lett. **105**, 242001 (2010).
- [41] X. Zhan et al. (2011), arXiv:1102.0318.
- [42] P. J. Mohr, B. N. Taylor, and D. B. Newell, Rev. Mod. Phys. **80**, 633 (2008).
- [43] R. Pohl et al., Nature **466**, 213 (2010).
- [44] S. J. Brodsky, C. E. Carlson, J. R. Hiller, and D. S. Hwang, Phys. Rev. Lett. **94**, 022001 (2005).
- [45] C. E. Carlson, V. Nazaryan, and K. Griffioen, Phys. Rev. A **78**, 022517 (2008).
- [46] C. E. Carlson, V. Nazaryan, and K. Griffioen, Phys. Rev. A **83**, 042509 (2011).
- [47] M. N. Rosenbluth, Phys. Rev. **79**, 615 (1950).
- [48] I. A. Qattan et al., Phys. Rev. Lett. **94**, 142301 (2005).
- [49] J. Arrington, Phys. Rev. C **69**, 022201(R) (2004).
- [50] Y. C. Chen, A. Afanasev, S. J. Brodsky, C. E. Carlson, and M. Vanderhaeghen, Phys. Rev. Lett. **93**, 122301 (2004).
- [51] J. Arrington, Phys. Rev. C **69**, 032201(R) (2004).
- [52] J. Arrington, D. M. Nikolenko, et al., Proposal for positron measurement at VEPP-3, arXiv:nucl-ex/0408020.
- [53] W. Brooks, A. Afanasev, J. Arrington, K. Joo, B. Raue, L. Weinstein, et al., Jefferson Lab experiment E04-116.
- [54] M. Kohl, AIP Conf. Proc. **1160**, 19 (2009).
- [55] P. G. Blunden, W. Melnitchouk, and J. A. Tjon, Phys. Rev. C **72**, 034612 (2005).
- [56] C. B. Crawford et al., Phys. Rev. Lett. **98**, 052301 (2007).
- [57] W. A. McKinley and H. Feshbach, Phys. Rev. **74**, 1759 (1948).
- [58] R. Gilman, A. Sarty, S. Strauch, et al., Jefferson Lab experiment E05-103.
- [59] J. Glister et al., Phys. Lett. **B697**, 194 (2011).
- [60] J. Alcorn et al., Nucl. Inst. & Meth. **A522**, 294 (2004).
- [61] G. Ron, J. Arrington, D. Day, R. Gilman, D. Higinbotham, A. Sarty, et al., *Measurement of the Proton Elastic Form Factor Ratio at Low  $Q^2$* , Jefferson Lab Experiment Proposal E08-007 (2008).
- [62] O. Gayou et al., Phys. Rev. C **64**, 038202 (2001).
- [63] X. Zhan, Ph.D. thesis, Massachusetts Institute of Technology (2010), arXiv:1108.4441.
- [64] J. Glister et al., Nucl. Instrum. Meth. **A606**, 578 (2009).
- [65] J. Arrington and I. Sick, Phys. Rev. C **70**, 028203 (2004).
- [66] J. Arrington (2011), arXiv:1108.3058.
- [67] J. C. Bernauer et al. (2011), arXiv:1108.3533.
- [68] D. Borisyuk and A. Kobushkin, Phys. Rev. **C75**, 038202 (2007).
- [69] G. A. Miller, Phys. Rev. C **66**, 032201 (2002).
- [70] S. Boffi et al., Eur. Phys. J. **A14**, 17 (2002).
- [71] A. Faessler, T. Gutsche, V. E. Lyubovitskij, and K. Pumsa-ard, Phys. Rev. D **73**, 114021 (2006).
- [72] E. L. Lomon (2006), arXiv:nucl-th/0609020.
- [73] M. A. Belushkin, H. W. Hammer, and U. G. Meissner, Phys. Rev. C **75**, 035202 (2007).
- [74] J. P. B. C. de Melo, T. Frederico, E. Pace, S. Pisano, and G. Salme, Phys. Lett. **B671**, 153 (2009).
- [75] E. L. Lomon, Phys. Rev. C **64**, 035204 (2001).
- [76] C. Crawford et al., Phys. Rev. **C82**, 045211 (2010).
- [77] D. Higinbotham, AIP Conf.Proc. **1257**, 637 (2010), arXiv:1001.3341.
- [78] I. Passchier, L. van Buuren, D. Szczerba, R. Alarcon, T. Bauer, et al., Phys.Rev.Lett. **88**, 102302 (2002).
- [79] B. D. Milbrath et al. (Bates FPP), Phys. Rev. Lett. **80**, 452 (1998).
- [80] B. D. Milbrath et al., Phys. Rev. Lett. **82**, 2221(E) (1999).
- [81] B. Hu, M. Jones, P. Ulmer, H. Arenhovel, O. Baker, et al., Phys.Rev. **C73**, 064004 (2006).
- [82] M. Paolone et al., Phys. Rev. Lett. **105**, 072001 (2010).
- [83] A. De Rujula, Phys.Lett. **B693**, 555 (2010).
- [84] I. C. Cloet and G. A. Miller, Phys.Rev. **C83**, 012201 (2011).
- [85] M. O. Distler, J. C. Bernauer, and T. Walcher, Phys.Lett. **B696**, 343 (2011).
- [86] B. Y. Wu and C. W. Kao (2011), arXiv:1108.2968.
- [87] G. Miller, A. Thomas, J. Carroll, and J. Rafelski (2011), arXiv:1101.4073.
- [88] V. Barger, C.-W. Chiang, W.-Y. Keung, and D. Marfatia, Phys. Rev. Lett. **106**, 153001 (2011).
- [89] U. Jentschura, Eur.Phys.J. **D61**, 7 (2011).
- [90] A. De Rujula, Phys.Lett. **B697**, 26 (2011).
- [91] R. J. Hill and G. Paz (2011), arXiv:1103.4617.
- [92] J. D. Carroll, A. W. Thomas, J. Rafelski, and G. A. Miller, AIP Conf. Proc. **1354**, 25 (2011), arXiv:1105.2384.
- [93] H. W. Hammer and U.-G. Meissner, Eur. Phys. J. **A20**, 469 (2004).
- [94] J. C. Bernauer, Ph.D. thesis, Johannes Guttenbert-Universitat Mainz (2010).
- [95] A. V. Volotka, V. M. Shabaev, G. Plunien, and G. Soff, Eur. Phys. J. **D33**, 23 (2005).